



Manganese(II) complexes of N,O-chelating dihydrazone: Synthesis, characterization, optical properties and corrosion inhibition on aluminum in HCl solution

A.M. Hassan^a, Ayman H. Ahmed^{a*}, Hosni A. Gumaa^a, Bassem H. Mohamed^b
and Ahmed M. Eraky^b

^aDepartment of Chemistry, Faculty of Science, Al-Azhar University, Nasr City, Cairo, Egypt

^bCairo Oil refining Company (CORC), Cairo, Egypt

ABSTRACT

Manganese(II) hydrazone complexes derived from condensation of oxaloyldihydrazide with salicylaldehyde and *o*-hydroxyacetophenone have been synthesized and characterized. The mode of bonding as well as the structure of the isolated compounds have been ascertained on the basis of data obtained from elemental analyses, spectral (UV-Vis., IR, mass, ¹H NMR), magnetism and thermal (TG and DTA) measurements. The dihydrazones hesitate in their coordination to the metal center in between pentadentate to tetradentate manner forming mononuclear (octahedral) and binuclear (tetrahedral) complexes, respectively. Optical transmission spectra were recorded in the range 190–2100 nm and some optical parameters such as band gap and refractive index have been determined. The inhibitive properties of all ligands for the corrosion of aluminum in 1 M HCl solutions were investigated using weight loss technique. The results pointed out that the two investigated ligands have reasonable inhibitions towards the corrosion of aluminum in acidic medium. The adsorption of the inhibitors on metal surface was found to be spontaneous first order reaction.

Keywords: Dihydrazone complexes; Spectroscopic studies; Band gap; Corrosion inhibition.

INTRODUCTION

Hydrazones and their derivatives constitute a versatile class of organic compounds that are important for drug design, organocatalysis and also for the syntheses of heterocyclic compounds [1]. In analytical chemistry hydrazones find application by acting as multidentate ligands [2] with metals (usually from the transition group). Indeed, hydrazones played a central role in the development of coordination chemistry. Hydrazones obtained by the condensation of *o*-hydroxy aldehydes with hydrazides are considered potential polynucleating ligands because they possess amide, azomethine and phenol functions thus offer a variety of bonding possibilities in metal complexes [3]. Extensive studies have revealed that the lone pair on trigonally hybridized nitrogen atom of the azomethine group is responsible for the chemical and biological activity [4-6]. Nevertheless, a lot of complexes derived from hydrazones [M= Cu(II), Ni(II), Pd(II), Co(II), V(IV), and ruthenium(II)] have been studied [7-14], little complexes of oxaloyldihydrazone ligands have been studied [15-17]. This is because oxaloyldihydrazones are soluble only in high polar solvents as DMF and DMSO which requires much effort to isolate them or their complexes in pure form. Worthy mention, some hydrazone complexes have been incorporated in zeolite-Y by analogous methods and the resulting materials were inferred by various physicochemical characterization techniques [18-22].

Most of the well-known acid inhibitors are organic compounds containing π bonds, phosphorus, sulfur, oxygen and nitrogen as well as aromatic rings in their structure which are the major adsorption centers [23]. The compounds containing both nitrogen and sulfur can provide excellent inhibition, compared with compounds containing only nitrogen or sulfur [24]. Generally, a strong interaction causes higher inhibition efficiency where the inhibition increases in the sequence $O < N < S$ [25]. Heteroatoms such as nitrogen, oxygen and sulphur are capable of forming coordinate covalent bond with metal owing to their free electron pairs and thus acting as inhibitor. Compounds with π -bonds also generally exhibit good inhibitive properties due to interaction of π orbital with metal surface. Different classes of organic compounds are used as corrosion inhibitors for metallic alloys in various acid media [26-28]. The first stage in the action mechanism of these organic inhibitors in aggressive acid media is their adsorption on the metal surface [29]. Unfortunately, many common corrosion inhibitors employed in aqueous media are health hazards [30].

The present work was carried out to report the synthesis and characterization of two oxaloyldihydrazones and their Mn(II)-complexes. The study was also extended to investigate the inhibition efficiency for used ligands on aluminum in hydrochloric acid pickling solution and some kinetic parameters have been determined. Moreover, the energy gap and refractive index of isolated ligands and complexes have been estimated to describe their optical and electronic properties.

EXPERIMENTAL ACTION

The selected metal salts, diethyl oxalate, hydrazine monohydrate were purchased from Sigma-Aldrich. The aldehydes were of E-Merck grade. Other chemicals and solvents were of highest purity and used without further purification. The ^1H NMR spectra were recorded on a Jeol-FX-90Q Fourier NMR spectrometer at 25 °C using DMSO solvent and TMS as an internal standard. Mass spectra of the ligands were performed by a Shimadzu-GC-MS-QP1000 EX using the direct inlet system. Metal contents (% wt) were estimated complexometrically by EDTA using xylenol orange as indicator and solid hexamine as buffer (pH = 6). Elemental analyses (CHN), spectral (UV-Vis., FT-IR) and thermal (TG, DTA) measurements were carried out as reported [31]. The optical band gap energy (E_g) of product compounds was calculated from Tuac's equations [32,33]. Aluminum specimen was of chemical compositions (wt %) depicted in Table 1. Prior to the experiment, the specimens were polished with emery papers (220-800 grades) until the surface appears free from any scratches and other apparent defects, then washed with distilled water followed by degreasing in absolute ethanol and acetone, dried at room temperature, weighed and finally stored in a moisture free desiccators prior to use.

Table 1. The characteristic specifications for aluminum coupon used for weight loss measurements.

Specimen	C	Si	As	Sn	Mn	P	S	Cr	Ni	Pb	Zn	Cu	Al	Fe
Aluminum	-	-	-	-	-	-	-	-	0.006	0.01	0.003	0.002	balance	0.27

2.2. Preparations

2.2.1 Preparation of oxalicydihydrazide

Oxalicydihydrazide ($\text{H}_2\text{NNHCO-CONHNH}_2$) was isolated by the reaction of diethyl oxalate (15 ml, 0.11 mole) and excess hydrazine monohydrate (9.8 ml, 0.22 mole) under continuous stirring in ice. The formed compound was filtered off, washed several times by water and ethanol, recrystallized from distilled water-ethanol mixed solvent including washing the solids repeatedly by ethanol to remove any excess of hydrazine. Finally, the isolated crystals were dried in oven at 80 °C for 8 hrs. The resulting product was melted at 240 °C (Lit. m.p = 240 °C) and is soluble in hot water and insoluble in alcohol.

2.2.2. Preparation of oxaloyldihydrazone ligands

The dihydrazone ligands; bis(salicylaldehyde)oxaloyldihydrazone (L_1) and bis(2-hydroxyacetophenone) oxaloyldihydrazone (L_2) were prepared by general condensation procedure. Oxalicydihydrazide (0.01 mol) dissolved first in hot water (20 cm^3) followed by adding methanol (40 cm^3) was mixed with the appropriate aldehydes [salicylaldehyde and 2-hydroxyacetophenone] (0.02 mol) in absolute methanol. The resulting mixture was refluxed for 3 hrs under constant stirring. The product separated out on concentrating the solution to half of its volume and cooling. The crystals of the desired ligand was collected by filtration through a Buchner funnel and dried in the oven at 50 °C for 2 h. After that the ligand was recrystallized from DMF-MeOH_{aq} mixed solvent it was collected, washed thoroughly on filter paper by acetone to remove any excess of DMF and then dried in an electric oven at 80 °C for 2

h. The authenticity of the two ligands was proved by elemental analyses, (IR, mass and ^1H NMR) spectroscopy (Table 2,3). The mass spectra of ligands (L_1, L_2) are shown in Fig. 1, and the M^+ values are listed in Table 2. Each of oxaloyldihydrazone exhibited one peak indicating the high purity of these compounds. The spectral data confirmed the chemical formula of the ligands as well the correct molecular weights.

2.2.3. Preparation of solid complexes

The dihydrazone ligand (1 mmol) was dissolved first in 20 ml DMF and then 50 ml methanol was added. The resulting solution was added slowly to a methanolic solution of Mn(II) acetate. The resulting mixture was heated under reflux for 4 hrs and then reduced to 30 cm³ by evaporation on hot plate adjusted at 50 °C. The resulting reaction mixture was cooled down to room temperature and the colored solid complexes were filtered off, washed several times with successive portions of hot solvents (dimethylformamide, methanol and acetone, respectively) to remove any excess of the unreacted ligand and finally dried in an electric furnace at 80 °C for 3 hrs.

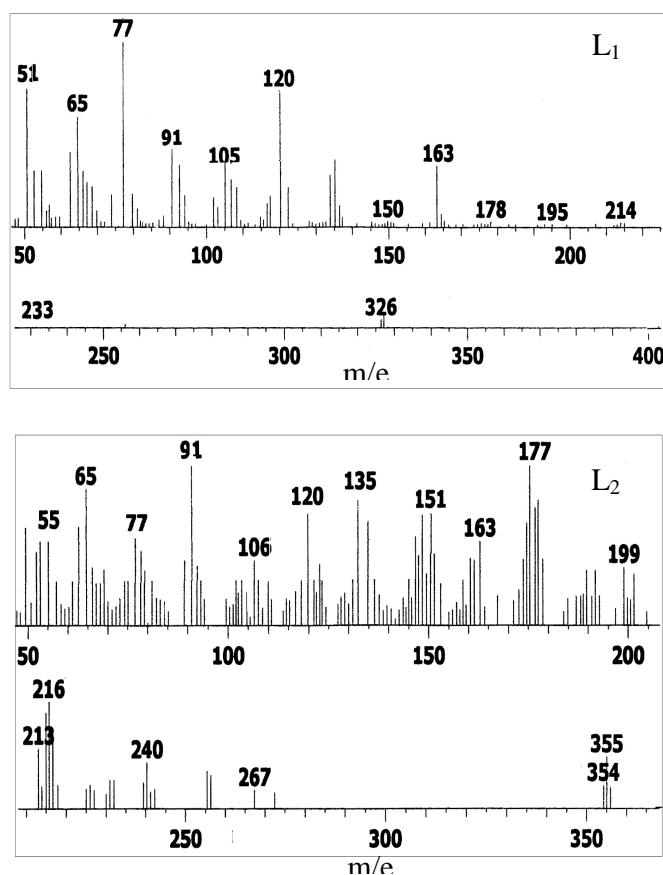


Fig.1. Mass spectra of L_1 and L_2

2.3. Corrosion inhibition of ligands

2.3.1 Weight loss measurement

In the weight loss experiment, 100 ml beakers containing 1M HCl solutions were employed at room temperature (28 °C). Stock solutions of the inhibitors were prepared in DMF. All test solutions contained 10 ml (20 vol.%) of DMF to maintain inhibitors completely soluble. The total volume of the test solution is 50 ml. The coupons were suspended in the beakers with the aid of glass hooks. In the absence of inhibitors, the coupons were retrieved from their corrodent solutions at 60 minutes interval for 240 minutes. Further measurements were carried out after introducing of the additives (L_1, L_3) at concentrations of 5×10^{-4} , 1×10^{-4} , 5×10^{-5} and 1×10^{-5} M for the same duration. Coupons were dipped into saturated ammonium acetate solution at room temperature, to terminate the corrosion reaction. They were washed by scrubbing with a light brush and dried in acetone and finally in an oven maintained

at 80 °C. The loss of weight of coupons is evaluated in grams as the difference in weight of the coupons before and after the test [34].

$$W = W_i - W_f$$

Where: W = weight loss of coupon, W_i = Initial weight of coupon, W_f = Final weight of coupon.

The value of corrosion rate, ρ (in $\text{gm.cm}^{-2}.\text{min}^{-1}$) was calculated from the following equation [35]:

$$\rho = W / A \times t$$

Where: W = weight loss to the nearest 0.0001gm, A = area of specimen to the nearest 0.01 cm^2 ($2 \times$ area of one surface/face) and t = exposure time (minutes).

The percentage inhibition efficiency (%IE), and a parameter surface coverage (θ) which represents the part of the surface covered by the inhibitor molecules, were calculated using the equations [35]:

$$\eta \% = [1 - \rho_1/\rho_2] \times 100\%$$

$$\theta = [1 - \rho_1/\rho_2]$$

Where: $\eta \%$ = corrosion inhibition efficiency, ρ_1 = corrosion rate in the presence of inhibitors, ρ_2 = corrosion rate in the absence of inhibitor at the same temperature and θ = surface coverage.

2.3.2. Kinetic treatment of weight loss results

The corrosion reaction is a heterogeneous one, composed of anodic and cathodic reactions with the same or different rate [36]. On this basis the kinetic analysis of the data is considered necessary. In the present study, the initial weight of steel coupon at time, t is designated W_i , the weight loss is ΔW and the weight change at time t is ($W_i - \Delta W$) or W_f . When $\log W_f$ was plotted against time, a linear variation was observed [37]:

$$\log W_f = \log W_i - Kt$$

Where: W_i = the initial weight before immersion, K = slope (the rate constant), and t is time.

From the rate constant values obtained from the graphs, the half-life values, $t_{1/2}$, of the metal in the test solutions were calculated using the equation [37]:

$$t_{1/2} = 0.693 / k$$

RESULTS AND DISCUSSION

The oxaloyldihydrazones (L_1 , L_2) and their solid complexes with Mn(II) have been isolated in a pure form. Physical, analytical and spectroscopic data of the hydrazones and their isolated complexes are given in Tables 2,3. The complexes are insoluble in H_2O , MeOH/EtOH, Et_2O , CHCl_3 , petroleum ether, acetone, CCl_4 as well as benzene meanwhile soluble in DMF and DMSO. Comparison of the elemental analysis for both the calculated and found percentages indicates that the compositions of the isolated solid complexes coincide well with the proposed formulae. Also the structure of the solid complexes have been identified on the basis of FT-IR, magnetism and UV-Vis. spectra. The solvent content of the complexes was determined by thermal (TGA and DTA) measurements and the results can be taken as evidence for the suggested structure.

Table 2. Analytical, physical and spectroscopic data of the oxaloyldihydrazones and their related metal complexes

Compd.	Symol	M.p(°C)	Found(Cald.)%				¹ H-NMR		μ_{eff}	M ⁺ Found/calcd.	E _g (eV)	Structure
		Color	C	H	N	M	Chemical shift (δppm)					
C ₁₆ H ₁₄ N ₄ O ₄	L ₁	>300	59.1	5.4	16.2	-	12.6(NH, s), 10.98(OH, s), 8.75(CH=N, s),	-	326.0/ 326.0	3.10	-	
		Yellow	(58.9)	(4.3)	(17.2)	-	6.6-8.40 (aromatic protons, m)					
C ₁₈ H ₁₈ N ₄ O ₄	L ₂	>300	59.5	6.1	14.7	-	12.85(NH, s), 11.85(OH, s), 6.6-8.0	-	356.4/354.2	3.32	-	
		Pale Yellow	(61)	(5.1)	(15.8)	-	(aromatic protons, m), 2.48(CH ₃ , s)					
[Mn(L ₁ -2H)(H ₂ O)].1.5H ₂ O	1	>300	44.8	3.9	13.0	14.0	-	4.5	-	2.83	Octahedral	
		Brownish	(45.3)	(4.0)	(13.2)	(13.0)						
[Mn ₂ (L ₃ -2H)(H ₂ O) ₂ (OAc) ₂].2H ₂ O	2	>300	40.0	4.3	8.1	17.1	-	4.8	-	2.64	Tetrahedral	
		Brown	(40.5)	(4.6)	(8.6)	(16.8)						

3.1. IR Spectra

The positions of the significant IR bands of dihydrazones and their manganese(II) complexes are summarized in Table 2.

Ligands: Oxaloyldihydrazones (L₁,L₂) can exist either in the trans (staggered) configuration or cis-configuration (anti-cis- or syn-cis-configuration), Fig. 2, [38]. NMR spectroscopy is considered a powerful technique employed to determine their skeleton. Infrared spectra of L₁ and L₂ showed strong bands at 1607 and 1620 cm⁻¹, respectively, assignable to the azomethine group (ν_{C=N}). The observation of these bands confirmed the interaction of dihydrazides with aldehydes forming azomethine linkages. The locations of ν(OH)_{phenolic/naphthoic}, ν(NH) and ν(C=O) for L₁ and L₂ were noticed at (3149, 3204 and 1666) and (3476, 3166 and 1705(m) +1660(v.s)), respectively. The appearance of both ν(C=O) and ν(NH) simultaneously in the IR spectra of L₁ indicates the presence of keto form. The appearance of carbonyl groups (C=O) near 1660 cm⁻¹ as one band in case of L₁ and two bands (1651, 1689 cm⁻¹) for L₂ indicates the trans (staggered-structure, Fig. 2) configuration for L₁ while mixture of [cis(syn/anti-cis-structure) + trans (staggered- structure), Fig. 2] isomers for L₂. This suggestion results from the field effect phenomenon which can be elucidated as follows. When 2C=O:: groups are in the same direction (cis configuration), the non-bonding electrons present on oxygen atoms cause electrostatic repulsion. This cause a change in the state of hybridization of C=O group and also make it to go out of the plane of the double bond. Thus, the configuration diminished and absorption occurs at higher wave number. Consequently, cis is absorbed (due to the field effect) at higher frequency compared to trans isomer. Subsequently, L₂ showed two bands for C=O, one of them (at high frequency) is associated to syn/anti-cis-structure while that at lower frequency related to staggered configuration. The low intensity of high frequency bands (near 1689 cm⁻¹) compared with that at low frequency (near 1651 cm⁻¹) indicates the domination of staggered structure. Worthy mention, NMR spectroscopy is in good agreement with this suggestion. The observation of OH (phenolic) group in L₁ at lower position (3149 cm⁻¹) is taken as evidence to the persistence of intermolecular H-bonding (O-H...N) between the phenolic-OH and azomethine group in solid state [39]. The proposition of intermolecular H-bond (O-H...O-H) between associated ligand molecules is excluded owing to the sharpness of this band. The remarkable downward frequency shift indicates the strength of this bond. In fact, ¹H NMR did not distinguish this H-bond in its spectra because execution of NMR analysis in high polar solvent (DMSO) led to break these bonds. The phenolic-OH group did not form H-bond in ligand L₂ where it is observed after 3400 cm⁻¹. Furthers, the existence of two bands at 3278 cm⁻¹ (L₁) may be attributed to ν(OH)_{enolic} in H-bond bonding with azomethine group. The lower shift for these two bands than the normal value asserts the weakness of this bond. The obscure of enolic OH in NMR spectra of L₁ may be due to two factors: (1) its lower concentrations. Minute molecules may change one or two of its C=O groups into enolized configuration but the keto form is still dominated, (2) dilution by high polar DMSO disrupted these H-bonds returning the modified molecules into keto forms. The significant ν(C-O) groups associated to the aromatic ring of the dihydrazones L₁ and L₂ were observed at 1275 and 1246 cm⁻¹, respectively [40]. Both investigated L₁ and L₂ dihydrazones ligands showed 3 bands at (1403, 1458, and 1486 cm⁻¹) and (1449, 1486 and 1512 cm⁻¹), respectively, assignable to ν(C=C) of the aromatic ring. Also, each ligand exhibited strong band in the region 700-800 cm⁻¹ corresponding to the out of plane deformation of the aromatic rings. The positions of other bands assigned to ν(CH)_{aliphatic} and ν(CH)_{aromatic} are shown in Table 3.

Table 3. Significant IR and electronic absorption data of oxaloyldihydrazones and their manganese complexes

Symbol	$\nu(\text{OH})$ phenolic (enolic)	$\nu(\text{H}_2\text{O})$	$\nu(\text{NH})$	$\nu(\text{C-H})$ aromatic (aliphatic)	$\nu(\text{C=O})$	$\nu(\text{C=N})$	$\nu(\text{C-O})$ phenolic	$\nu(\text{OAc})$	$\delta(\text{C-H})$ aromatic out of plane	$\nu(\text{M-O})$ phenolic/enolic/ carbonyl	λ_{max} , nm (assignments)
L ₁	3149 (3278)	-	3204	3062 (2924)	1666	1620	1275	-	756	-/-/-	390(n- π^* , C=N), 350(n- π^* , C=O), 340(π - π^* , C=N), 303(π - π^* , C=O), 292(π - π^* , Phenyl)
L ₂	3448 (-)	-	3293	3048 (2923)	1689 1651	1607	1246	-	746	-/-/-	372(n- π^* , C=N), 352(n- π^* , C=O), 336(π - π^* , C=N), 305(π - π^* , C=O), 290(π - π^* , Phenyl)
1	- (3350)	3370 merged	3204 shoulder	3020 (2928)	1666	1606	1284	-	757	592/508/-	525 (${}^6\text{A}_{1g} \rightarrow {}^3\text{T}_{1g}$) (G) 430 (${}^6\text{A}_{1g} \rightarrow {}^2\text{T}_{2g}$) (G)
2	3329 (-)	3414	-	3057 (2924)	1689	1602	1242	1363 1471	751	562/-/-	490 (${}^6\text{S} \rightarrow {}^4\text{G}$) 425 (${}^6\text{S} \rightarrow {}^4\text{P}$)

Mn(II) complexes: the dihydrazones L₁ and L₂ in their complexes are coordinated to the central metal ion in penta and tetradentate manner forming mono and binuclear complexes, respectively. This various behavior of ligands can be explicated from the IR data set out in (Table 3). The mode of bonding in complexes can be identified by comparing IR spectra of complexes with that of the related ligand as follows.

For complex 1, the structural formula is proposed on the basis: (1) the negative shift of the azomethine group to lower wavenumber asserted the involvement of this group in bonding [41]. This negative shift of $\nu(\text{C=N})$ bond is attributed to a decrease in the π -bond character of the $-\text{C=N}$ group as a result of nitrogen to metal coordination. (2) The positive shift observed for $\nu(\text{C-O})$ vibrations ($1275 \rightarrow 1284 \text{ cm}^{-1}$) simultaneously with obscure of $\nu(\text{OH}_{\text{phenolic}})$ indicated the deprotonation of phenolic (OH) during coordination [42]. (3) Appearance of both $\nu(\text{NH})$ and $\nu(\text{C=O})$ as weak intensity shoulders without any shift in their positions is most probable due to the obscure of one NH and one C=O groups by virtue of enolization effect. This happened due to the enolization of left or right half of the dihydrazone molecule assuming keto-enol skeleton. (3) Noticeable of $\nu(\text{OH}_{\text{enolic}}, 3350 \text{ cm}^{-1})$ and $\nu(\text{M-OH}_{\text{enol}}, 508 \text{ cm}^{-1})$ reflected the undeprotonation of the enolic (OH) group during the coordination [43]. For complex 2, the unshift of the azomethine (C=N) group compared with free L₂ ligand asserted the uninvolved of this group in bonding. Interestingly, the obscure of $\nu(\text{NH})$ band with noticeable of $\nu(\text{C=O})$ band at 1689 cm^{-1} upon chelation indicates the keto form of L₂ giving a conclusive evidence to the coordination of metal ion with deprotonated NH group. Foundation of C=O as one band in 2 instead of two bands in free L₂ besides its absorption at somewhat higher frequency, 1689 cm^{-1} , is most probable due to the presence of the two oxygen atoms related to (O=C-C=O) in cis direction because of the field effect. On the other hand, the lower shift of $\nu(\text{OH}_{\text{phenolic}})$ and shift $\nu(\text{C-O})$ by 119 and 4 cm^{-1} , respectively, besides issuing of $\text{M-O}_{\text{phenolic}}$ at 562 cm^{-1} , upon complexation sustained bonding of metal ion with phenolic (OH) group but without deprotonation. Doubtless the appearance of new M-O bands in two Mn(II)-complexes (Table 3) confirms the formation of metal-ligand complexes. Furthermore, crystalline and coordinated water in 1 and 2 species assumed on the appearance of the broad bands within the range $3300\text{--}3450 \text{ cm}^{-1}$. Further, compound 2 containing acetate group showed two bands in the region 1363 cm^{-1} and 1471 cm^{-1} , suggesting ν_{as} and ν_{s} carboxylic modes, respectively. The larger difference between the $\nu_{\text{as}}(\text{OAc})$ and $\nu_{\text{s}}(\text{OAc})$ frequencies is an indicative of monodentate nature of acetate group. Finally, the slight changes in the positions of $\nu(\text{C=C})_{\text{ph}}$ of free ligands upon chelation [complex 1($1410, 1439, 1468, 1572 \text{ cm}^{-1}$) and complex 2 ($1438, 1490$ and 1522 cm^{-1})] resulted from metal-ligand interaction.

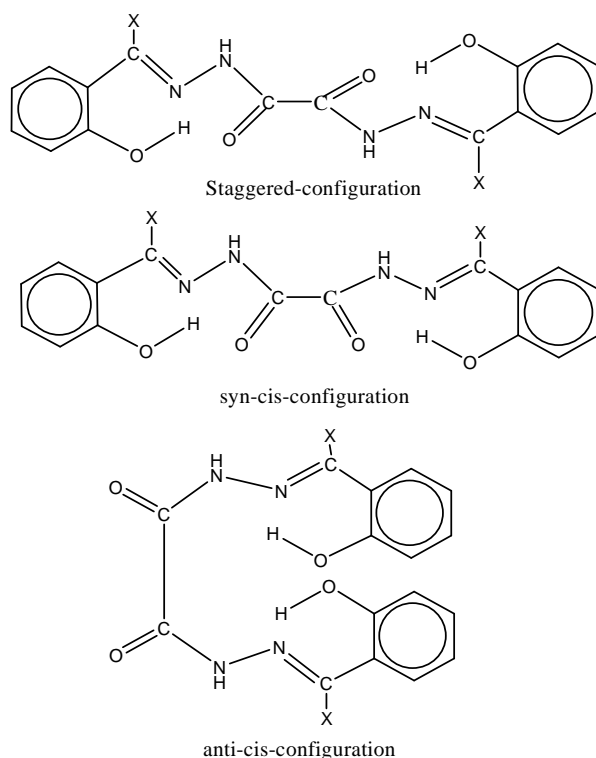


Fig. 2. Proposed structures of L_1 ($X=H$) and L_2 ($X=CH_3$)

3.2. 1H NMR Spectra

The assignment of the main signals in 1H NMR spectra of the two ligands are given in Table 2.

1H NMR spectra of L_1 and L_2 ligands exhibited multiple signals of the aromatic protons in the 6.5–8.5 ppm region. The signals of equal integration observed in L_1 and L_2 at δ (12.6, 11) and (12.9, 11.8) ppm downfield of TMS have been assigned to NH and ortho-OH protons, respectively. Upon the addition of D_2O then OH and NH signals were obscured. Further, the existence of the δOH (phenolic/naphthoic) at its normal frequency excluded any intramolecular hydrogen bonding operating between ortho-OH group and the azomethine group ($C=N\dots H-O$). The azomethine signals, $\delta(CH=N)$, observed only in L_1 has been assigned at 8.75 ppm. As reported in literature [43,44], if the dihydrazone exists in the syn-cis-configuration or staggered configuration, the δOH , δNH and $\delta CH=N$, resonances, each should appear as a singlet. However, the appearance of these signals in the form of six signals (doublet of doublet) indicates anti-cis (chair) configuration. Actually, the features of the 1H NMR spectra of the dihydrazones are in consistent with the syn-cis- or staggered configuration. According to IR interpretation mentioned above, the staggered configuration is well defined/dominated for used ligands. 1H NMR spectrum of L_2 differs from that of L_1 where the former revealed signals at 2.55 ppm downfield of TMS due the methyl (CH_3) protons, respectively [10].

3.3. Electronic spectra and magnetic studies

The assignments of the observed electronic absorption bands of the oxaloylhydrazones and their metal complexes as well as the magnetic data of the formed chelates are shown in Table 3. The electronic data of the studied ligands in DMF exhibited five absorption bands at λ_{max} (nm) equals 350-392 ($n-\pi^*$, $C=N$), 338-375 ($n-\pi^*$, $C=O$), 306-340 ($\pi-\pi^*$, $C=N$), 292-315 ($\pi-\pi^*$, $C=O$) and 280-303 ($\pi-\pi^*$, aromatic ring). The essential features of the spectrum of the complex are entirely different when compared to that of the free ligand, which supports the coordination of the ligands to the metal ions. The electronic spectra of complex 1 in DMF showed two weak bands at 525 and 430 nm assignable to $^6A_{1g} \rightarrow ^4T_{1g}(G)$ and $^4T_{2g}(G)$ transitions, respectively, suggesting an octahedral configuration around the Mn^{2+} ions [45]. Complex 2 revealed two absorptions at 490 and 425 nm (but appears as strong compared with complex 1 spectrum) assigned to $^6S \rightarrow ^4G$ and 4P transitions, respectively. The observation of these bands suggests a tetrahedral

configuration around Mn^{II} ion [46]. Other transitions attributed to octahedral (${}^6A_{1g} \rightarrow {}^4E_g$, ${}^4A_{1g}$, ${}^4T_{2g}(D)$ and ${}^4E_g(D)$) and tetrahedral (${}^6S \rightarrow {}^4D$ and 4F) $Mn(II)$ geometries are masked by strong ligand bands [45].

The μ_{eff} value of complex 1, which contains one metal ion, is close to spin only value and is considered to be in good consistent with the proposed structure. For other consequential binuclear complex (2), the magnetic moment values are less than that expected per molecular formula regarding the existence of two metal ions in the proposed structures. This can be explained on the basis of metal-metal interaction. It is suggested that this complex has high spin but presence of two metals near to each other in the same molecule may cause partial quenching of the spin moments of the metal ions (spin coupling) decreasing the magnetism [47]. This means that the supposition of two metal ions in the molecular structure is not excluded and the obtained μ_{eff} values may be not conflicted with the proposed structures.

3.4. Thermal stability

To examine the thermal stabilities of Mn^{II} -complexes, thermal gravimetric analyses (TGA) and differential thermal analysis (DTA) for metal complexes were carried out. The TGA and DTA curves of complex 1 gave four stages of disintegration. The first one (50-220 °C) corresponds to the elimination of ($H_2O_{\text{coordinated}} + 1.5 H_2O_{\text{crystalline}}$, found/calculated = 11.5/10.6%). The other three stages detected at 220-400, 400-500 and 800-870 °C point to the gradual decomposition of the complex with formation of $MnO/MnCO_3$ mixture at the final stage (found/calculated = 16.6/16.7)%. DTA curve is in good agreement with TG thermogram. It exhibited one endothermic peak at nearly 70 °C corresponding to the loss of crystalline water as well as four exothermic peaks at mid point 200, 370, 480 and 825 °C relating to the complex degradation.

TG curve of complex 2 revealed four stages of decomposition. The first stage (50-100 °C) concerns the loss of $2H_2O_{\text{crystalline}}$ (found/calculated = 6.2/5.5)% and accompanied by endothermic peak in DT curve. The other three decomposition stages observed in TG curve at 150-320, 320-400 and 400-520 °C refer to the gradual decomposition of the complex with formation of $Mn/MnCO_3$ residue at the last stage (found/calculated = 26.0/26.3)%. The resulting metal (Mn) associated with the final stage is eventuated by the reduction of metal oxide by released carbon. These TG stages are accompanied by three exothermic peaks at mid points 250, 400 and 420 °C supporting the TG results.

In the light of the forgoing results, the likely structures of the metal complexes can be represented by Fig. 3.

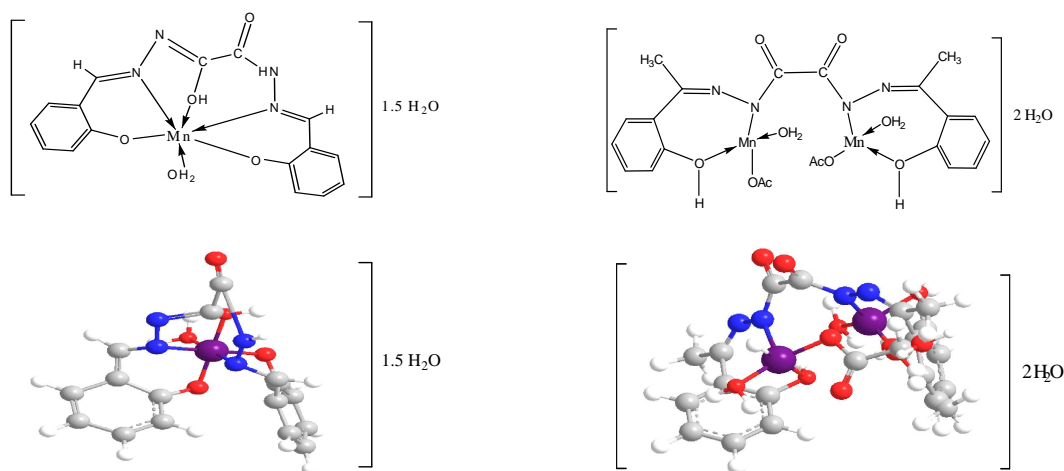


Fig. 3. Suggested structures of Mn^{II} -oxaloyldihydrazone complexes

3.5. Optical properties

The optical and the electrical properties of metals complexes have recently interesting due to great potential application in Schottky diode, solid state devices and optical sensor [48]. For this purpose the optical band gap (E_g) of oxaloyldihydrazone ligands and their $Mn(II)$ complexes have been calculated from the following equations:

The measured transmittance (T) was used to calculate approximately the absorption coefficient (α) using the relation

$$\alpha = 1/d \ln(1/T)$$

where d is the width of the cell, T is the measured transmittance. The optical band gap was estimated using Tuac's equations [32,33]:

$$\alpha h\nu = A (h\nu - E_g)^m$$

where m is equal to 1/2 and 2 for direct and indirect transition, respectively, A is an energy independent constant.

The values of α calculated from the first equation was used to plot $(\alpha h\nu)^2$ vs. $h\nu$ (Fig. 4) from which an indirect band gap was found by extrapolating the linear portion of the curve to $(\alpha h\nu)^2 = 0$. The values of indirect optical band gap E_g were determined and given in Table 2. The E_g values of oxaloyldihydrazone ligands and Mn(II)-complexes in DMF solvent were found to be at 3.10-3.32 and 2.64-2.83 eV, respectively as indicated in Fig. 4 and Table 2. Inspection of Table 2 reveals that the optical band gap values of the two ligands (E_g) have been reduced upon complexation. As reported in literature [49] it is suggested that after complexation, metal leads to raise mobilization of the ligand electrons by accepting them in its shell. It can be evaluated that after formation of the complex, the chemical structure of the ligands is changed, the width of the localized levels is expanded and in turn, the band gap is smaller. This result is very significant in applications of electronic and optoelectronic devices, because of the lower optical band gap of the materials [50]. Small band gap facilitates electronic transitions between the HOMO-LUMO energy levels and makes the molecule more electro-conductive [51]. In essence, the obtained band gap values suggest that these complexes are semiconductors and lie in the same range of highly efficient photovoltaic materials. So, the present compounds could be considered potential materials for harvesting solar radiation in solar cell applications [49,52]. Perhaps, the little difference in the optical band gap E_g values between two studied complexes is due to their synonymous chemical structures.

The evaluation of refractive indices of optical materials is of considerable importance for applications in integrated optic devices such as switches, filters and modulators. Besides, the refractive index is an important physical parameter, which is widely used in chemistry to identify the liquid, or its purity. For this purpose, optical properties were investigated for the compounds by spectrophotometric measurement of transmittance, T, and reflectance, R, at normal incidence in the wavelength range of 190–900 nm. The optical reflectance spectra (R) for oxaloyldihydrazone ligands and their Mn(II) complexes as a function of wavelength (λ , nm) are shown in Fig. 5. The reflectance has been estimated using the relationship, $R+T+A=1$, for normal reflectance, the refractive index value (n) of the compounds may be approximately expressed by the relation [53],

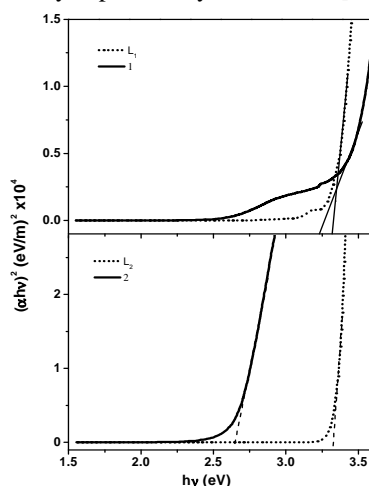


Fig. 4. The plots of $(\alpha h\nu)^2$ vs. $h\nu$ of Mn(II)-oxaloyldihydrazone complexes

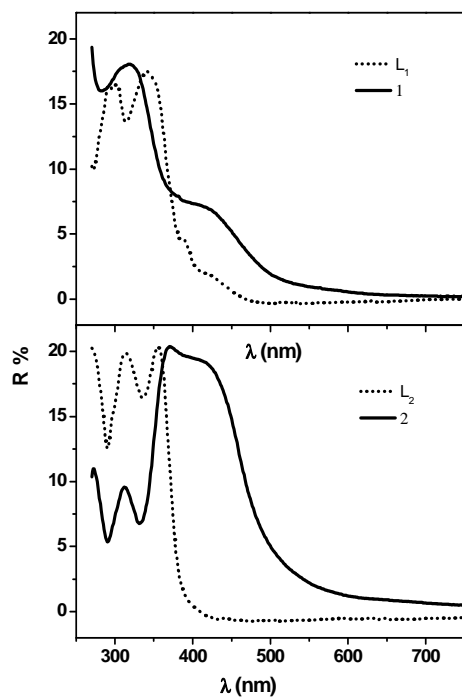


Fig. 5. The optical reflectance spectra (R) for oxaloyldihydrazone ligands and their Mn(II) complexes

$n = (1 + \sqrt{R}) / (1 - \sqrt{R})$, where R is the normal reflectance.

The variations in the refractive index (n) with wavelength (λ , nm) is shown in Fig. 6. The variation of n values with frequency range indicates that some interactions take place between photons and electrons [48]. Moreover, Fig. 6 indicates that the complexation affects the refractive index of the free ligands where there is a difference in the n values upon connection.

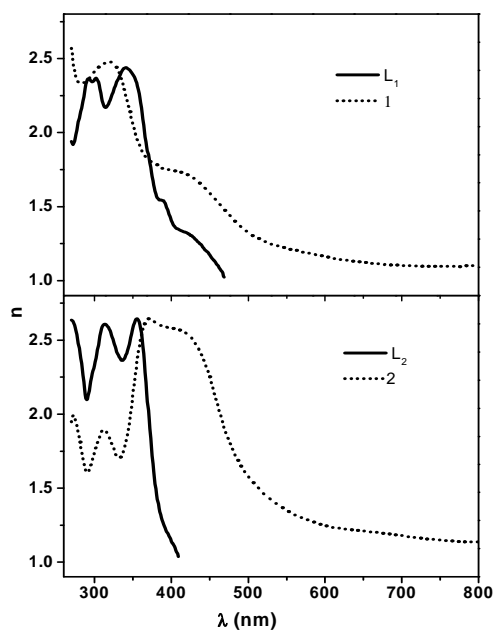


Fig. 6. The variation of the refractive index (n) with wavelength (λ) for oxaloyldihydrazone ligands and their Mn(II) complexes

3.6. Corrosion inhibition

Weight loss data of aluminum in 1M HCl in the absence and presences of various concentrations of inhibitors were obtained and are given in Table 4. It is obvious from this table that the weight loss decreases as the concentrations of different compounds increase. Also, it was observed that inhibition efficiencies increase with increase in inhibitor concentrations. This behavior resulted from the adsorption of hydrazones on the metal coupons/solution interface where the adsorbed species mechanically screen the coated part of the metal surface from the action of the corrosive medium. This adsorption could be attributed to physico-chemical properties of the investigated ligands molecules as functional groups (OH, NH, C=O and C=N), quite large molecular size, high molecular weight, aromaticity, electron density at the donor atoms (N:, :O:) and also the π -orbital character of azomethine, carbonyl and phenyl groups. Adsorption and desorption of inhibitor molecules continuously occur at the metal surface and an equilibrium exists between the two processes at a particular temperature. The order of inhibition efficiency of hydrazone compounds is: $L_2 > L_1$ and this trend can be interpreted on the basis of the electron donating nature of methyl group attached to the azomethine ($-N=C(CH_3)$) which increases the electron density on the azomethine group causing high bond strength between the ligand and metal surface. The order of increasing inhibition efficiency of the hydrazide derivatives are depicted in Table 4 for aluminum in 1 M HCl. The obtained data, Fig. 7, indicates a convincing evidence for the application of the used ligands as corrosion inhibitors. The maximum efficiency for L_1 and L_2 are 49 and 50%, respectively, which indicates an acceptable inhibition for aluminum.

Table 4. Corrosion parameters for aluminum coupons in (1M HCl) solution in presence and absence of different concentrations of hydrazone ligands obtained from weight loss measurement at room temperature after 4 hrs immersion time

Inhibitor	Conc. (M)	Weight Loss (g)	Rate of corrosion $mg\ cm^{-2}\ h^{-1}$	θ	Inhibition efficiency $\eta\ %$	K $(day^{-1}) \times 10^{-3}$	$t_{1/2}$ (days) $\times 10^2$
L_1	Blank	0.0609	0.0203	-	-	94.4	0.07
	5×10^{-4}	0.0312	0.0104	0.49	49	47.9	0.14
	1×10^{-4}	0.0354	0.0122	0.40	40	54.5	0.13
	5×10^{-5}	0.0426	0.0149	0.26	26	65.7	0.11
	1×10^{-5}	0.0460	0.0153	0.24	24	71.0	0.10
L_2	Blank	0.0327	0.0109	-	-	52.4	0.13
	5×10^{-4}	0.0162	0.0054	0.50	50	25.8	0.27
	1×10^{-4}	0.0192	0.0066	0.39	39	30.6	0.23
	5×10^{-5}	0.0215	0.0075	0.31	31	34.3	0.20
	1×10^{-5}	0.0236	0.0079	0.28	28	37.7	0.18

Efficiency (%)

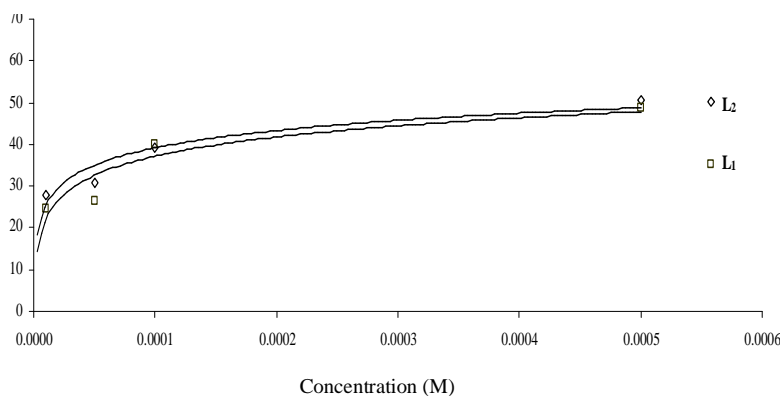


Fig. 7. The efficiency for aluminum coupons in 1M HCl solution in the presence and absence of different concentrations of oxaloyldihydrazone ligands at room temperature

3.6.1. Kinetic considerations

Regarding the experimental section, when $\log W_f$ was plotted against time, Fig. 8, for aluminum sheets in the presence of oxaloyldihydrazone ligands, a linear variation was observed, which confirmed first-order reaction

kinetics with respect to the abovementioned sheet in HCl solutions [54]. Table 4 gives the rate constants and half life values. There is a general decrease in the rate constants with increasing concentrations of oxaloyldihydrazone inhibitors, Table 4. The increment of half-life ($t_{1/2}$) with increase in concentration of dihydrazone ligands refers to the inhibition of aluminum in 1M HCl by the additives. The increase in half life indicates more protection of the metals by the oxaloyldihydrazone ligands [50].

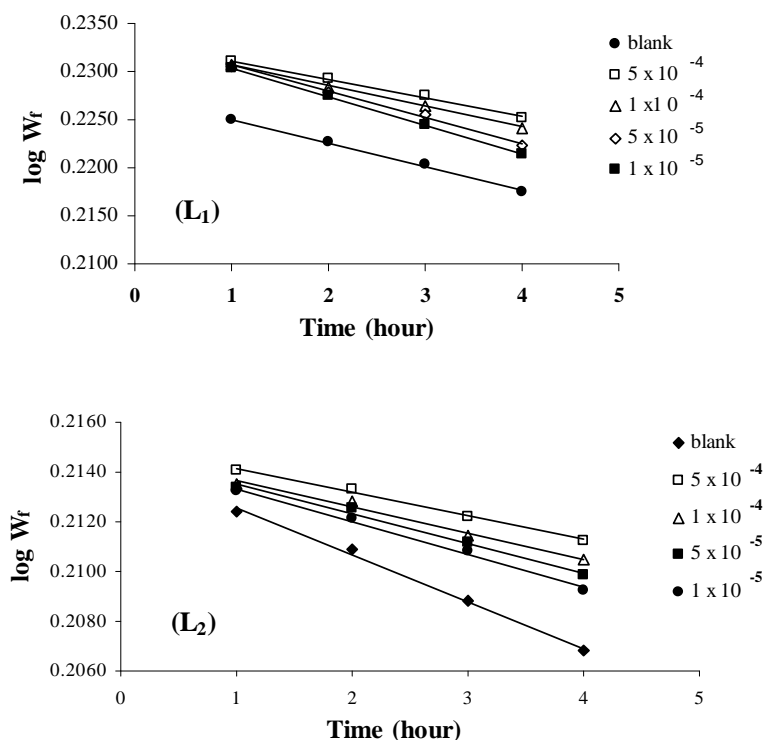


Fig. 8. Variation of $\log W_f$ with time (hour) for aluminum coupons in HCl solution containing oxaloyldihydrazone ligands (L_1, L_2)

CONCLUSION

Two oxaloyldihydrazone ligands (L_1 and L_2), was prepared essentially by the usual condensation reaction between oxaloyldihydrazide and the appropriate aldehyde (salicylaldehyde and 2-hydroxyaceto-phenone) in 1:2 molar ratio. The formed compounds were purified by crystallization to give bis(salicylaldehyde)oxaloyldihydrazone (L_1) and bis(2-hydroxyacetophenone)oxaloyldihydrazone (L_2). The separated oxaloyldihydrazones can react with acetate solution of Mn(II) ion to produce solid Mn(II) complexes. Comparison the elemental analysis for both the calculated and found percentages indicates that the compositions of the isolated solid complexes coincide well with the proposed formulae. Elemental analyses (CHN), UV-Vis, FT-IR spectroscopy and ^1H NMR spectra emphasized the formation of the desired complexes (1,2). The dihydrazone is bonded in complex 1 as keto-enol pentadentate ligand through phenolate oxygen, azomethine nitrogen and one deprotonated enolized carbonyl (C-OH) giving mononuclear complex. In complex 2, it acts as a diketo tetradentate ligand through phenolic oxygen and deprotonated secondary NH giving binuclear complex. The presented physico-chemical and spectral data suggested an octahedral geometry for complex 1 and tetrahedral symmetry for complex 2. The indirect band gap energy (E_g) for all separated compounds lies in the range of semiconductor materials. The results of corrosion inhibition presented in this paper revealed the ability of ligands to inhibit the corrosion of aluminium in HCl solutions. The inhibition efficiency of the inhibitors increases with increasing of ligand concentration and the adsorption of the inhibitors on metal surface follows spontaneous first order reaction.

REFERENCES

[1] P Barbazan; R Carballo; B Covelo; C Lodeiro; JC Lima; EM Vazquez-Lopez; *Eur. J. Inorg. Chem.*, **2008**, 2713–2720.

- [2] LH Terra; AMC Areias; I Gaubeur; MEV Suez-Iha; *Spectrosc. Lett.*, **1999**, 32, 257.
- [3] EM Sherif, AH Ahmed, *Synth. React. Inorg. Met.-Org. Chem.*, **2010**, 40, 365–372.
- [4] M Ghasemian; A Kakanejadifard; F Azarban; A Zabardasti; S Shirali; Z Saki; S Kakanejadifard; *Spectrochim. Acta*, **2015**, 38, 643–647.
- [5] AH Ahmed; E Ewais; *J. Chem. Pharm. Res.*, **2012**, 4(7), 3349–3360.
- [6] JM Price; *Federation Proc.*, **1961**, 20(3), 223–226.
- [7] VP Singh; A Katiyar; *Pestic. Biochem. Phys.*, **2008**, 92(1), 8–14.
- [8] VP Singh; P Singh; AK Singh; *Inorg. Chim. Acta*, **2011**, 379(1), 56–63.
- [9] M Challaa; TS Reddy; *African Journal of Pure and Applied Chemistry*, **2011**, 5(13), 442–447.
- [10] H Abd El-Wahab, M Abd El-Fattah, AH Ahmed, AA Elhenawy, NA Alian, *J. Organomet. Chem.*, **2015**, 791, 99–106.
- [11] V Lozan; PG Lassahn; C Zhang; B Wu; C Janiak; G Rheinwald; H Lang; *Z Naturforsch., B* **2003**, 58, 1152.
- [12] WH Hegazy; *Monatsh. Chem.*, **2001**, 132, 639.
- [13] R Dinda; P Sengupta; S Ghosh; TCW Mak; *Inorg. Chem.*, **2002**, 41, 1684.
- [14] R Raveendran; S Pal; *Polyhedron*, **2005**, 24, 57.
- [15] M Salavati-Niasari; A Sobhani; *J. Mol. Catal.*, **2008**, 285, 58–67.
- [16] RA Lal; S Adhikari; A Kumar; J Chakraborty; S Bhaumik; *Synth. React. Inorg. Met.-Org. Chem.*, **2002**, 32(1), 81–96.
- [17] RA Lal; D Basumatary; S Adhikari; A Kumar; *Spectrochim. Acta*, **2008**, 69(3), 706–714.
- [18] A.H. Ahmed, *Rev. Inorg. Chem.*, **2014**, 34(3), 153–175.
- [19] AH Ahmed; MS Thabet; *Syn. and Rea. in Ino. and Metal-Org. Chem.*, **2015**, 45, 1632–1641
- [20] AH Ahmed; AG Mostafa; *Mate. Sci. Eng., C*: **2009**, 29(3), 877–883.
- [21] AH Ahmed; MS Thabet; *J. Mol. Struct.*, **2011**, 1006, 527–535.
- [22] MS Thabet; AH Ahmed; *J. Porous Mater.*, **2013**, 20, 319–330.
- [23] R Lopez-Sesenes; JG Gonzalez-Rodriguez; M Casales; L Martinez; JC Sanchez-Ghenno; *Int. J. Electrochem. Sci.*, **2011**, 6, 1772–1784.
- [24] J Aljourani; MA Golozar; K Raeissi; *Mater. Chem. Phys.*, **2010**, 121(1-2), 320–325.
- [25] HS Awad; SA Gawad; *Anti-Corros. Method Mater.*, **2005**, 52(6), 328–336.
- [26] F Bentiss; M Traisnel; H Vezin; HF Hildebrand; M Lagrenee; *Corros. Sci.*, **2004**, 46(11), 2781–2792.
- [27] EA Noor; *Corros. Sci.*, **2005**, 47(1), 33–55.
- [28] X Li; L Tang; L Li; G Mu; G Li; *Corros. Sci.*, **2006**, 48(2), 308–321.
- [29] IL Rozenfeld; *Corrosion Inhibitors*, McGraw–Hill Inc., **1981**.
- [30] EW Flick; *Corrosion Inhibitors*, Park Ridge, New Jersey, **1987**.
- [31] TM Salama; AH Ahmed; ZM El-Bahy; *Micropor. Mesopor. Mater.*, **2006**, 89, 251–259.
- [32] MM Rashad; AM Hassan; AM Nassar; NM Ibrahim; A Mourtada; *Appl. Phys., A* **2013**, 117, 877–890.
- [33] MM Rashad; AO Turkey; AT Kandil; *J. Mater. Sci.: Mater. Electron.*, **2013**, 24, 3284–3291.
- [34] K Orubite-Okorosaye; NC Oforka; *J. Appl. Sci. Environ-Mgt.*, **2004**, 8(1), 57–61.
- [35] IA Mohammed-Dabo; SA Yaro; G Abubakar; SI Ayilara; TU Apugo-Nwosu; SA Akuso; *J. Basic. Appl. Sci. Res.*, **2011**, 1, 1989–1999.
- [36] AO Jamesv O Akaranta; *African Journal of Pure and Applied Chemistry*, **2009**, 3(12), 262–268.
- [37] PC Okafor; EE Ebenso; UJ Ekpe; *Int. J. Electrochem. Sci.*, **2010**, 5, 978–993.
- [38] RA Lat; S Adhikari; A Kumar *In. J. Chem.*, **1997**, 36A, 1063–1067.
- [39] K Burger; I Ruff; F Ruff; *J. Inorg. Nucl. Chem.*, **1965**, 27, 179–190.
- [40] OB Chanu; A Kumar; A Ahmed; RA Lal; *J. Mol. Struct.*, **2012**, 1007, 257–274.
- [41] AM Ali; AH Ahmed; TA Mohamed; BH Mohamed; *Transit. Met. Chem.*, **2007**, 32, 461–467.
- [42] OB Chanu; A Kumar; A Ahmed; RA Lal; *J. Mol. Struct.*, **2012**, 1007, 257–274.
- [43] A Kumar; RA Lal; OB Chanu; R Borthakur; A Koch; A Lemtur; S Adhikari; S Choudhury; *J. Coord. Chem.*, **2011**, 64(10), 1729–1742.
- [44] RA Lal; D Basumatary; J Chakraborty; S Bhaumik; A Kumar; *Ind. J. Chem.*, **2006**, 45, 619–628.
- [45] FA Cotton; G Wilkinson; *Advanced Inorganic Chemistry*, 2Ed, Interscience, **1966**.
- [46] C Furlani; G Furlani; *J. Inorg. Nucl. Chem.*, **1961**, 19, 51–58.
- [47] BB Mahapatra; SK Kar; *J. Ind. Chem. Soc.*, **1991**, 68, 542–544.
- [48] XT Tao; H Suzuki; T Watanabe; SH Lee; S Miyata; H Sasabe; *Appl. Phys. Lett.*, **1997**, 70, 1503–1505.
- [49] F Karipcin; B Dede; Y Caglar; D Hur; S Ilcan; M Caglar; Y Sahin; *Opt. Commun.*, **2007**, 272, 131–137.
- [60] N Turan; B Gündüz; H Korkoca; R Adigüzel; N Çolak; K Buldurun; *J. Mex. Chem. Soc.*, **2014**, 58(1), 65–75.
- [51] SK Sengupta; OP Pandey; BK Srivastava; V Sharma; *Transit. Met. Chem.*, **1998**, 23, 349–353.

[52] ML Fu; GC Guo; X Liu; LZ Cai; JS Huang; *Inorg. Chem. Commun.*, **2005**, 8, 18-21.

[53] JI Gittleman; EK Sichel; Y Arie; *Sol. Energy Mater.*, **1997**, 1, 93-104.

[54] AO James; O Akaranta; *African Journal of Pure and Applied Chemistry*, **2009**, 3 (12), 262-268.